THE JOURNAL OF BIOLOGICAL CHEMISTRY VOL. 286, NO. 35, pp. 31003–31013, September 2, 2011
Printed in the U.S.A.

L-Ala-γ-D-Glu-*meso*-diaminopimelic Acid (DAP) Interacts Directly with Leucine-rich Region Domain of Nucleotide-binding Oligomerization Domain 1, Increasing Phosphorylation Activity of Receptor-interacting Serine/Threonine-protein Kinase 2 and Its Interaction with Nucleotide-binding Oligomerization Domain 1*

Received for publication, May 3, 2011, and in revised form, July 8, 2011 Published, JBC Papers in Press, July 12, 2011, DOI 10.1074/jbc.M111.257501

Hamed Laroui[‡1], Yutao Yan[‡], Yoshie Narui[§], Sarah A. Ingersoll[‡], Saravanan Ayyadurai[‡], Moiz A. Charania[‡], Feimeng Zhou[¶], Binghe Wang[‖], Khalid Salaita[§], Shanthi V. Sitaraman[‡], and Didier Merlin[‡2]**

*From the [‡]Department of Medicine, Division of Digestive Diseases and [§]Department of Chemistry, Emory University, Atlanta, Georgia 30322, [¶]Department of Chemistry and Biochemistry, California State University, Los Angeles, California 90032, [‖]Department of Chemistry, Georgia State University, Atlanta, Georgia 30302-4098, and **Veterans Affairs Medical Center, Decatur, Georgia 30033*

The oligopeptide transporter PepT1 expressed in inflamed colonic epithelial cells transports small bacterial peptides, such as muramyl dipeptide (MDP) and L-Ala-γ-D-Glu-*meso*-diaminopimelic acid (Tri-DAP) into cells. The innate immune system uses various proteins to sense pathogen-associated molecular patterns. Nucleotide-binding oligomerization domain (NOD)-like receptors of which there are more than 20 related family members are present in the cytosol and recognize intracellular ligands. NOD proteins mediate NF-κB activation via receptor-interacting serine/threonine-protein kinase 2 (RICK or RIPK). The specific ligands for some NOD-like receptors have been identified. NOD type 1 (NOD1) is activated by peptides that contain a diaminophilic acid, such as the PepT1 substrate Tri-DAP. In other words, PepT1 transport activity plays an important role in controlling intracellular loading of ligands for NOD1 in turn determining the activation level of downstream inflammatory pathways. However, no direct interaction between Tri-DAP and NOD1 has been identified. In the present work, surface plasmon resonance and atomic force microscopy experiments showed direct binding between NOD1 and Tri-DAP with a K_d value of 34.5 μM. In contrast, no significant binding was evident between muramyl dipeptide and NOD1. Furthermore, leucine-rich region (LRR)-truncated NOD1 did not interact with Tri-DAP, indicating that Tri-DAP interacts with the LRR domain of NOD1. Next, we examined binding between RICK and NOD1 proteins and found that such binding was significant with a K_d value of 4.13 μM. However, NOD1/RICK binding was of higher affinity (K_d of 3.26 μM) when NOD1 was prebound to Tri-DAP. Furthermore, RICK phosphorylation activity was increased when NOD was prebound to Tri-DAP. In conclusion, we have shown that Tri-DAP interacts directly with the LRR domain of NOD1 and consequently increases RICK/NOD1 association and RICK phosphorylation activity.

Commensal bacteria that colonize the human colon produce significant amounts of di/tripeptides. We were the first to report that PepT1 transports the small formylated bacterial peptide (fMLP) (1, 2). In the interval since that time, we have shown that other bacterial peptides, such as MDP[3] and Tri-DAP, may also be transported by hPepT1 (3, 4). Small bacterial peptides occur at substantially lower levels in the small intestine compared with the colon in line with the reduced numbers of prokaryotes present in the small intestine of humans. Interestingly, hPepT1 expression is normally restricted to the small intestine, a site in which the levels of small bacterial peptides are low, reflecting the sparse bacterial load of this tissue relative to that of the colon. Thus, the profile of hPepT1 expression along the normal human digestive tract is such that access of small bacterial peptides to hPepT1 minimizes intracellular uptake of these peptides. This normal expression pattern becomes altered in patients with chronic ulcerative colitis or Crohn disease in whom expression of hPepT1 occurs in the colon. The transporter will consequently mediate the intracellular accumulation of small prokaryotic materials. We and others have shown that such accumulation of bacterial products (including

* This work was supported, in whole or in part, by National Institutes of Health Grants RO1-DK-071594 and RO1-DK-55850 from the NIDDK (to D. M.) and Grant P20-MD001824-01 from the Research Infrastructure in Minority Institutions Program at California State University, Los Angeles and Grant SC1MS070155-01 from the NINDS (to F. Z.). This work was also supported by the Department of Veterans Affairs.

We dedicate this article to the memory of Dr. Shanthi V. Sitaraman, a brilliant scientist, dedicated physician, passionate humanitarian, and dearest friend.

[1] To whom correspondence should be addressed: Dept. of Medicine, Division of Digestive Diseases, 615 Michael St., Atlanta, GA 30322. Tel.: 404-727-6234; Fax: 404-727-5767; E-mail: hlaroui@emory.edu.

[2] Recipient of a senior research award from the Crohn's and Colitis Foundation of America.

[3] The abbreviations used are: MDP, muramyl dipeptide; DAP, diaminopimelic acid; NOD, nucleotide-binding oligomerization domain; AFM, atomic force microscopy; SPR, surface plasmon resonance; LRR, leucine-rich region; NOD1, NOD type 1; NOD2, NOD type 2; RICK (or RIPK), receptor-interacting serine/threonine-protein kinase 2; CARD, caspase-activating domain; mDeg, millidegrees; RIU, refractive index units; RU, resonance units; CM, circulating molecule.

Tri-DAP, fMLP, and MDP) may trigger intracellular signals that initiate intestinal inflammatory responses (3, 5–8).

In addition to maintaining efficient physical and biological barriers, the intestinal epithelium takes an active part in inducing both the innate and adaptive immune systems. Sensing the presence of a pathogen is the first step in mounting the effective immune response required for elimination of the invading organism and establishing protective immunity. The innate immune system uses various molecules to sense pathogen-associated molecular patterns. NOD-like receptors of which over 20 related family members exist are present in the cytosol and recognize intracellular ligands (9–13). NOD proteins mediate NF-κB activation (9–13). The specific ligands for some NOD-like receptors have been identified. NOD1 is activated by peptides that contain a diaminophilic acid, such as the PepT1 substrate Tri-DAP, whereas NOD2 recognizes muramyl dipeptides including the PepT1 substrate MDP. However, direct binding between NOD1 and Tri-DAP or NOD2 and MDP has not been demonstrated. In other words, PepT1 transport activity plays an important role in determining the intracellular loading levels of potential ligands for NOD1 and NOD2; this in turn determines the activation levels of downstream inflammatory pathways (9–13). NOD1 is expressed principally by antigen-presenting cells and epithelial cells that are exposed to microorganisms (14). NOD1 consists of a C-terminal leucine-rich region (LRR), a central NOD region, and an N-terminal caspase-activating domain (CARD) (14). NOD1 signaling has been shown to activate NF-κB and mitogen-activated protein kinases (14). Such signaling is presumably initiated by detection of NOD1 ligands by the LRR domain of NOD1 followed by recruitment of the downstream effector molecule, RICK (14) (see Fig. 1*A*). RICK is a CARD-containing serine/threonine kinase that physically binds to NOD1 via a CARD/CARD interaction (14) (see Fig. 1*A*). In the present study, we explored a possible direct interaction between Tri-DAP and NOD1 and the consequence of this binding on downstream effector molecules involved in inflammatory pathways. The mechanism by which NOD1 receptors sense small bacterial products may cause a predisposition to intestinal inflammation; however, specific hypotheses remain to be formulated.

Herein we used AFM and surface plasmon resonance (SPR) techniques to investigate the binding between NOD1 and Tri-DAP. AFM data indicated that the height of the NOD1 protein layer increased by a value commensurate with the thickness of Tri-DAP, suggesting association of the tripeptide with the NOD1 protein. SPR data showed a direct binding constant between two molecules (NOD1 protein and Tri-DAP oligopeptide) or between a molecule (RICK kinase) and a molecular complex (NOD1·Tri-DAP).

EXPERIMENTAL PROCEDURES

Cell Culture—Caco2-BBE cells were cultured to confluence in 75-cm^2 flasks at 37 °C in a humidified atmosphere containing 5% (v/v) CO_2. The culture medium was DMEM/Ham's F-12 medium (Invitrogen) supplemented with L-glutamine (2 mM), penicillin (100 units/ml), streptomycin (100 μg/ml), and heat-inactivated fetal calf serum (10%, v/v) (Atlanta Biologicals, Atlanta, GA).

RNA Extraction and Quantitative Real Time RT-PCR—Total RNA was extracted using the TRIzol reagent (Invitrogen) and reverse transcribed using a first strand cDNA synthesis kit (Fermentas, Glen Burnie, MD). Quantitative RT-PCR was performed using the SYBR Green qPCR Master Mix (Fermentas) and a Mastercycler Realplex (Eppendorf, Hamburg, Germany). The 18 S RNA and GAPDH housekeeping genes were used for controls, and -fold induction was calculated by the Ct method as follows: $\Delta\Delta Ct = (Ct_{Target} - Ct_{housekeeping})_{group\ 1} - (Ct_{Target} - Ct_{housekeeping})_{group\ 2}$; the final data were derived from $2^{-\Delta\Delta Ct}$. The primers used were as follows. The NOD1 primers were 5′-TCC AAA GCC AAA CAG AAA CTC-3′ (sense) and 5′-CAG CAT CCA GAT GAA CGT G-3′ (antisense), the GAPDH primers were 5′-GTC GGA GTC AAC GGA TTT GG-3′ (sense) and 5′-AAG CTT CCC GTT CTC AGC CT-3′ (antisense), and the 18 S RNA primers were 5′-CCC CTC GAT GAC TTT AGC TGA GTG T-3′ (sense) and 5′-CGC CGG TCC AAG AAT TTC ACC TCT-3′ (antisense).

Western Blotting—Recombinant proteins (NOD1, truncated NOD1 (Novus Biologicals, Littleton, CO), and RICK (Sigma)) were resolved by SDS-PAGE and transferred to polyvinylidene difluoride membranes (Bio-Rad). As all recombinant proteins were GST-tagged, membranes were probed for 1 h at room temperature with anti-human GST tag antibody (Cell Signaling Technology, Boston, MA). *In vitro* experiments of NOD1 Western blot were performed using an anti-mouse NOD1 antibody (Abnova, Walnut, CA). After washing, membranes were further incubated for 1 h at room temperature with appropriate horseradish peroxidase-conjugated secondary antibodies (Amersham Biosciences). Immunoreactive proteins were detected using an enhanced chemiluminescence system (Amersham Biosciences).

NOD1 SiRNA Transfection with Lipofectamine 2000—For each 12-well plate, 40 pmol of siRNA were dissolved in 100 μl of Opti-MEM. Either NOD1 siRNA or scrambled siRNA (from Ambion, Austin, TX) was mixed with 100 μl of Opti-MEM containing 5 μl of Lipofectamine. Cells were incubated with this mixture for 24 h. Next, cells were washed with PBS and placed in DMEM containing 5 mM Tri-DAP for 1, 2, or 4 h. The medium was collected for ELISA analysis of IL-8 levels.

ELISA—The ELISA detecting IL-8 was performed according to the manufacturer's protocol (R&D Systems, Minneapolis, MN).

AFM Measurement—All AFM measurements were performed with a JEOL instrument (JSPM-4210 scanning probe microscope, JEOL, Tokyo, Japan) equipped with ultrasharp contact mode cantilevers (MikroMasch, San Jose, CA) with a spring constant that ranged from 0.01 to 0.08 newton/m. To find the thickness of the adsorbed protein layers, the AFM tip was first used to remove molecules from the gold-coated carboxydextran chip surfaces by repeatedly scanning the same region with a high set point (+10.0 V) and rapid scan rate (~100 Hz). The scan size was limited to a region of 500 × 500 nm, and these settings were selected to ensure that all soft matter was removed, thus exposing the underlying gold substrate and revealing the *z*-position of the solid support. To check that the AFM tip reached the surface, the films were scratched for

different durations, and the resulting depths were measured under low force conditions. To passively image the thickness of the protein layer without introducing any scratches, the set point was reduced to 0.0 V, the scan area was increased to 2–4 μm^2, and the scan speed was reduced (~5.8 Hz). To account for surface variation within each chip and to acquire data amenable to statistical evaluation, topographical images were acquired from four different areas of the coated chip. The thickness of a chip coated with carboxydextran (only) was used as a reference (thus, $z = 0.0$ nm). Note that the tip was exchanged frequently to minimize the possibility of tip damage and tip wear due to excessive force application.

Preparation of Gold Chips Used to Detect SPR—For SPR experiments, we used gold films coated onto BK7 glass slides (Biosensing Instruments, Tempe, AZ). Each chip is a glass surface coated with a gold layer (47 nm thick) over an intermediate layer of chromium (2 nm in thickness). After each gold chip was cleaned with pure ethanol and dried under a stream of N_2, 15–20 μl of cystamine dihydrochloride (20 mM; Sigma) was cast onto each film overnight in a humidified reaction chamber. Cystamine dihydrochloride is light-sensitive, and the chamber was thus covered with a lid. Next, each chip surface was thoroughly rinsed with deionized water and dried by gentle blowing with a stream of N_2 (15).

We prepared a fresh mixture of 15 mM *N*-hydroxysuccinimide, 75 mM 1-ethyl-3-(3-dimethylaminopropyl) carbodiimide, and 6 mg/ml carboxymethyldextran (Sigma) and added this mixture to chips modified with cystamine dihydrochloride followed by incubation in a humidified chamber for at least 3–5 h (often overnight). We next rinsed and dried each chip surface under a stream of N_2 (15).

After placing a chip into the BI-2000 SPR machine, we coated NOD1 onto a gold film after preactivation with 1-ethyl-3-(3-dimethylaminopropyl) carbodiimide/*N*-hydroxysuccinimide solution. This step was repeated until the NOD1 coating level permitted the conduct of SPR experiments (Δ ~60–80 mDeg). Two fluidic channels can be used on this instrument, and the same sample plug flowed from the first to the second channel. When "serial mode" is selected, the BI-2000 machine coats simultaneously both channels with the same amount of NOD1. This option is essential to permit comparison of the interaction between NOD1 and RICK in the presence or absence of Tri-DAP. Residual activated carboxyl groups were neutralized by a final injection of 1 mM ethanolamine (Sigma). For analysis, a first injection of Tri-DAP was followed by RICK injection with "single mode" selected on channel 1. For comparison, the same protocol was used in the absence of Tri-DAP, again selecting single mode on channel 2.

Calculation of Association Constants—SPR is based on excitation and detection of the collective oscillations of free electrons in a metal film. Such electron oscillations are termed surface plasmons. A light is focused on the film through a glass prism, and reflected light is detected. At the resonance angle, plasmons absorb light, and a dark line is seen in the reflected beam. Any molecular binding event taking place on or near the metal film causes a shift in the resonance angle. By assessing shift over time, molecular binding events can be monitored, and the kinetics of binding events can be analyzed without the use of labels.

Several different units have been used to describe SPR signals. The most common include angular shift in degrees, refractive index units (RIU), and resonance units (RU) (16). Angular shift in degrees is the shift in resonance angle upon molecular adsorption or change in the refractive index of the solution. RIU reflect a change in solution refractive index or development of any other process inducing an alteration in SPR signal equivalent to a variation in RIU. RU reflect adsorption at a chip surface that causes a change in an SPR signal. One RU is equivalent to 1 pg/mm^2 of sensor surface. The three parameters may be interconverted as follows: 10^{-6} RIU = 0.73 RU = 7.3×10^{-5} degree = 0.73 pg/mm^2; 0.1 mDeg = 1 pg/mm^2. Conversion from mDeg or RU to RIU assumes the use of a buffer with an index of refraction close to 1.33, a BK7 prism, and a gold-coated sensor chip.

Association and dissociation constants of interactions between NOD1 (full length) or LRR-truncated NOD1-coated molecules and RICK, Tri-DAP, or MDP circulating molecules (CMs) were obtained using a BI-2000 (Biosensing Instruments) using SPR theory. K_d values (expressed in mol/liter^{-1}), which measure the 50% adsorption levels of CMs onto gold chips covered with coated molecules, are commonly used to describe the affinity between two molecules, such as how tightly a ligand binds to a particular receptor. Ligand-receptor affinities are influenced by non-covalent intermolecular interactions between the two molecules, including hydrogen-bonding, electrostatic interactions, and hydrophobic and Van der Waals forces. Briefly, after coating a chip with NOD1 or LRR-truncated NOD1, CM solutions of increasing concentration were passed over the chip. A two-step interaction curve was obtained. The first step involved adsorption of CMs to the maximal level. In the second step, when the flow of CM concentration returned to zero, nonspecific adsorbed CMs are released with the running buffer. On the chip, only coated molecule remained "attached." The adsorption curve kinetics thus decreased to a plateau located at a level above the initial base line. The amplitude of CM binding to coated molecules was taken to be the difference between the initial and final levels. K_d values were next determined by analysis of the binding curves obtained using different concentrations of CMs.

Kinase Assay—The LANCE Ultra TR-FRET (PerkinElmer Life Sciences) assay uses the proprietary W1024 europium chelate donor dye in combination with ULight, a low molecular weight acceptor dye showing a red shift in fluorescence emission upon binding. In a typical LANCE assay, phosphorylation of a ULight-peptide substrate is detected using a specific anti-phosphopeptide antibody labeled with europium chelate. Binding of the europium chelate-labeled phosphopeptide antibody to a phosphorylated ULight-peptide brings the donor and acceptor molecules into spatial proximity. Upon irradiation of the reaction solution at 320 or 340 nm, energy emitted by the excited europium chelate donor is transferred to nearby ULight acceptors, which next emit a signal at 665 nm. The intensity of light emission is proportional to the level of ULight substrate phosphorylation. Results are presented as signal/background ratios of fluores-

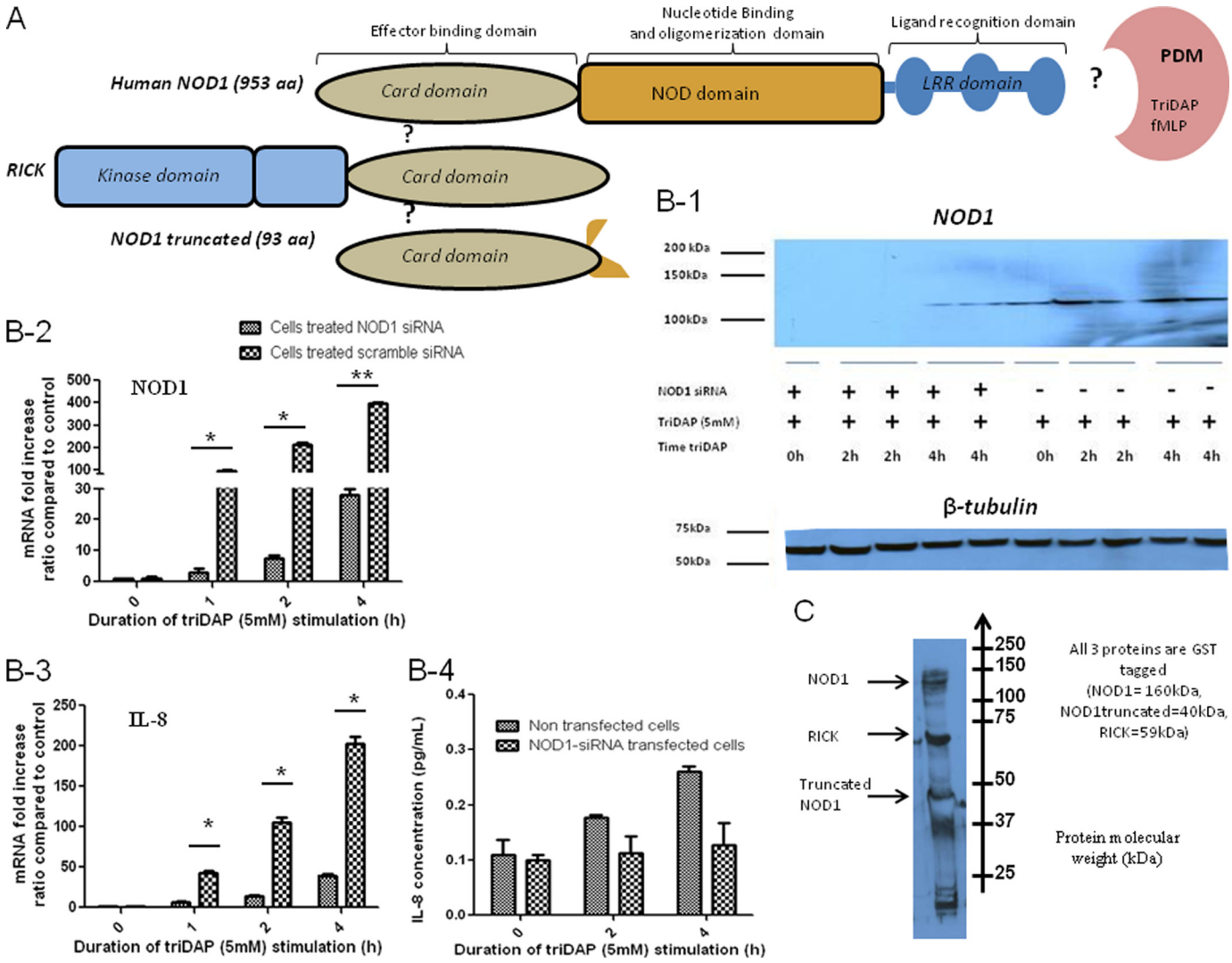

FIGURE 1. **NOD1 expression is essential for intestinal inflammation induced by hPepT1-mediated Tri-DAP transport.** *A*, schematic representation of possible direct interactions between Tri-DAP/NOD1 and NOD1/RICK. *B*, Western blotting analysis of NOD1 (*B-1*) in Caco2-BBE cells stimulated or not by Tri-DAP for 2 or 4 h. β-Tubulin was used as a control of protein loading. The levels of mRNA encoding NOD1 (*B-2*) and IL-8 (*B-3*) were measured by RT-PCR. IL-8 protein levels in the supernatants of Caco2-BBE cells stimulated or not by Tri-DAP for 1, 2, or 4 h were determined by ELISA (*B-4*). *C*, Western blotting analysis of interactions between NOD1-GST, RICK-GST, and NOD1-GST without the LRR domain. The values represent means ± standard error (S.E.) of $n = 3$/group. *, $p < 0.05$; **, $p < 0.01$. *aa*, amino acids.

cence resonance energy transfer (FRET) fluorescence (signal at 665 nm/control value (minus signal from ATP at 665 nm).

Statistical Analysis—Data are expressed as means ± S.E. Statistical analysis was performed using the unpaired two-tailed Student's *t* test featured in inStat version 3.06 (GraphPad) software. $p < 0.05$ was considered statistically significant.

RESULTS AND DISCUSSION

NOD1 Expression Is Essential for Intestinal Inflammation Induced by hPepT1-mediated Tri-DAP Transport—Previously, we showed that hPepT1 efficiently transports the tripeptide Tri-DAP into the interior of human intestinal epithelial cells inducing an inflammatory response via interaction with NOD1. The response activated the NF-κB inflammatory pathway that in turn stimulated IL-8 secretion (6, 17–20). To explore the importance of NOD1 in the proinflammatory signaling pathway activated by PepT1-mediated Tri-DAP transport (21), we down-regulated NOD1 expression using an siRNA approach. As shown in Fig. 1*B-1*, NOD1 expression (protein) in Caco2-BBE cells transfected with siRNA directed against NOD1 was knocked down. Some NOD1 protein expression was apparent after 4 h of Tri-DAP (5 mM) stimulation; however, these levels were decreased compared with cells that were not transfected with NOD1 siRNA. Also as shown in Fig. 1*B-1*, Tri-DAP induced NOD1 protein expression after 2- and 4-h stimulation of Caco2-BBE cells. Similarly in Fig. 1*B-2*, NOD1 mRNA expression in Caco2-BBE cells transfected with siRNA directed against NOD1 was reduced by 93% after 4 h of Tri-DAP-mediated induction compared with the expression level in untransfected cells or those transfected with scrambled siRNA. Next, we showed that down-regulation of intestinal NOD1 in intestinal epithelial Caco2-BBE cells due to siRNA treatments reduced the enhancement in expression of IL-8 seen upon exposure to 1 mM Tri-DAP for 2 or 4 h. Thus, IL-8-encoding mRNA decreased 5-fold, whereas the protein level dropped by 2-fold. The resulting levels of IL-8-encoding mRNA and pro-

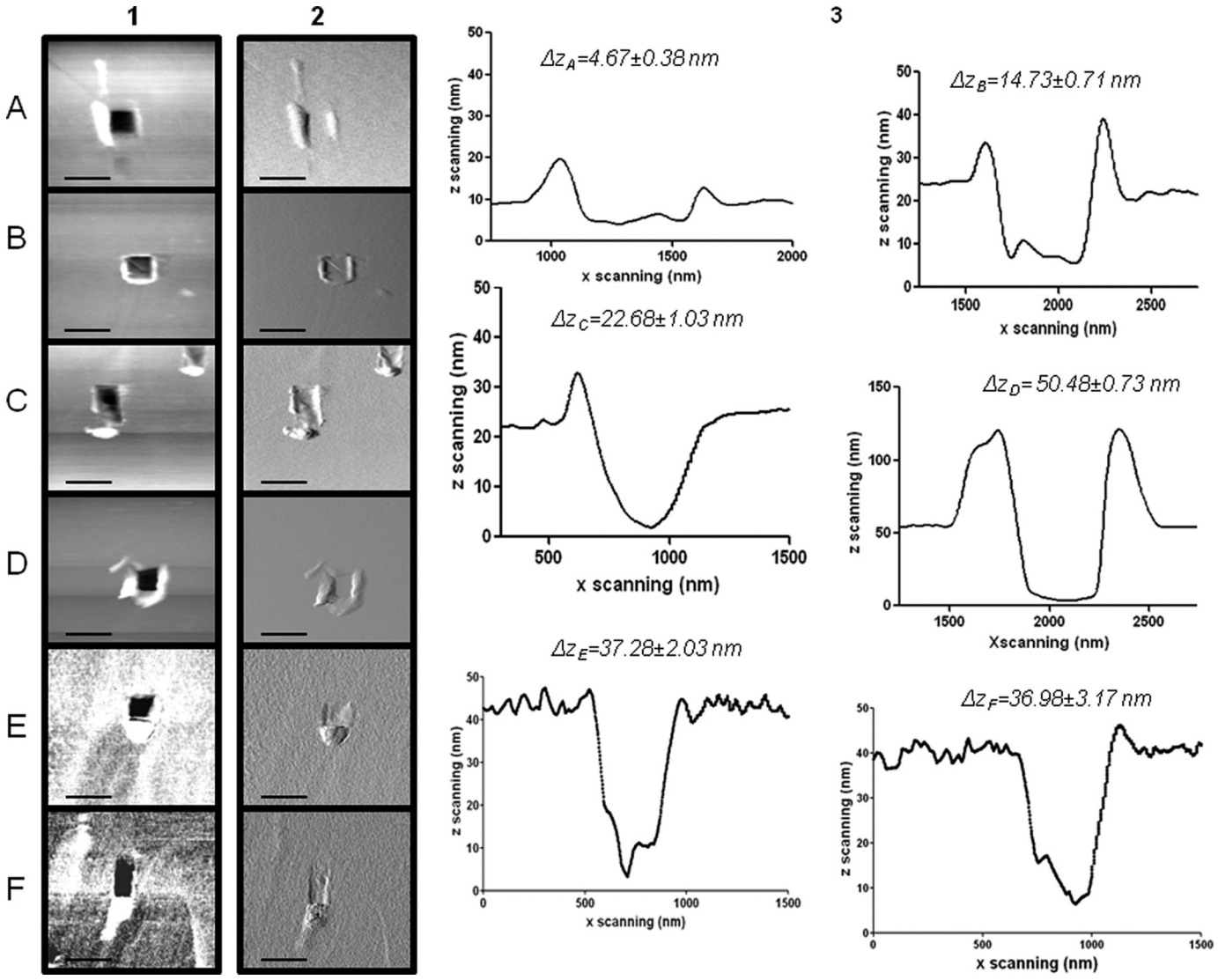

FIGURE 2. **Effective covalent binding of NOD1 to gold chip and molecular multilayer establishment measured by AFM.** *Column 1* contains topographical data, and *column 2* contains frictional force information on the multilayer containing interacting molecules. *Column 3* shows the thicknesses of the multilayer complex formed by various molecular combinations. *Row A* represents carboxydextran bound to a gold surface (4.67 ± 0.38 nm), *row B* represents carboxydextran/NOD1 (14.73 ± 0.71 nm), *row C* represents carboxydextran/NOD1/Tri-DAP (22.68 ± 1.03 nm), *row D* represents carboxydextran/NOD1/Tri-DAP/RICK (50.48 ± 0.73 nm), *row E* represents carboxydextran/LRR-truncated NOD1/Tri-DAP (37.28 ± 2.03 nm), and *row F* represents carboxydextran/LRR-truncated NOD1 (36.98 ± 3.17 nm). *Scale bar*, 500 nm. Representative micrographs and traces from four independent experiments are shown.

tein were comparable with those of unstimulated Caco2-BBE cells (Fig. 1, *B-3* and *B-4*, respectively). These experiments demonstrate that NOD1 is essential for activity of the proinflammatory signaling pathway activated by PepT1-mediated transport of Tri-DAP (4). However, these experiments did not provide direct evidence of binding between molecules involved in the pathway. To study direct protein/protein interactions, we obtained recombinant proteins that are known to be involved in the signaling pathway (Fig. 1*C*).

Effective Binding of NOD1 to Gold Chip and Interaction with Tri-DAP and RICK as Measured by AFM—In the present work, AFM was used to explore the possibility of a direct interaction among NOD1, Tri-DAP, and RICK that could be subsequently confirmed via SPR. The AFM tip scratch method (22) was used to measure the thickness of the adsorbed protein film upon exposure to solutions of protein that associated with NOD1. Specifically, we repeatedly scanned (100–1,000 scans) a region of interest (500 × 500 nm^2) applying high force loads to remove protein and to measure the z position of the underlying gold layer ($z = 0$). Next, the cantilever was retracted, and routine AFM imaging of a larger area (2–4 μm^2) was used to measure z', the thickness of the protein-coated layer in the vicinity of the scratched region. In Fig. 2, *column 1* shows the topography, whereas *column 2* contains data derived from lateral force microscopy. The topography channel provides quantitative information on the height of objects scanned by the AFM tip. The second signal, lateral force microscopy, is a measure of tip bending in the lateral direction. Such bending is the result of several factors including friction, force dissipation, surface rigidity, and molecular roughness. Here, lateral force microscopy data also reflect interactions with the meniscus as the work was conducted under ambient conditions. Fig. 2, *column*

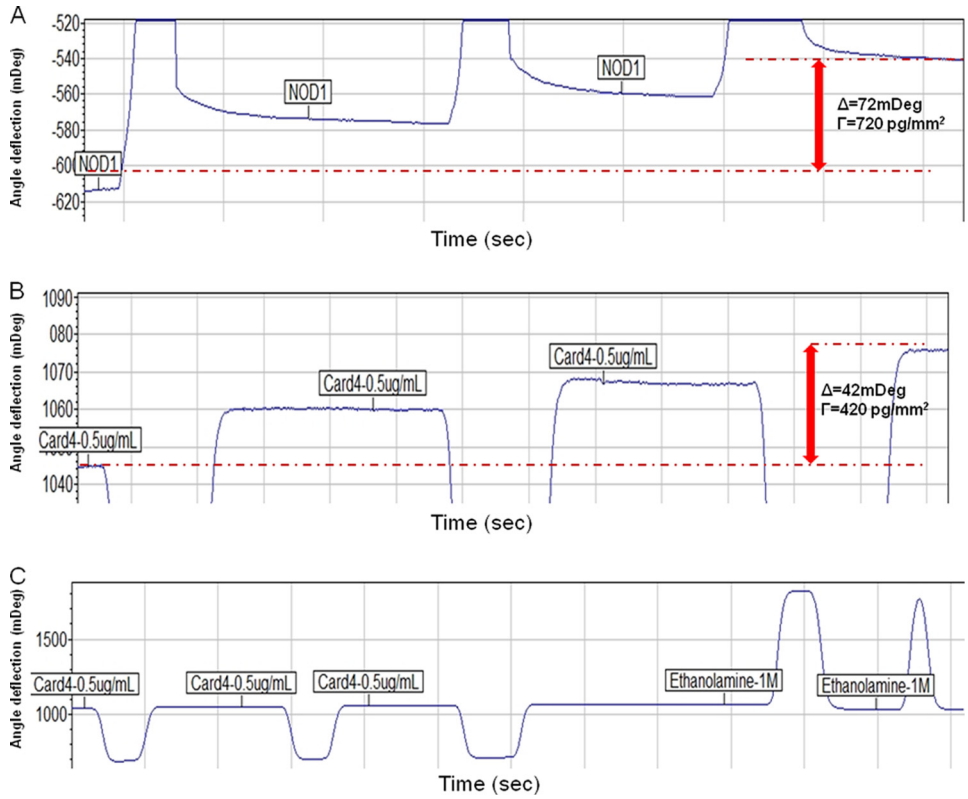

FIGURE 3. **Immobilization of NOD1 and NOD1 without LRR domain on carboxydextran sensor chip.** A sensorgram shows adsorption of NOD1 (*A*) or LRR-truncated NOD1 (*B*) onto carboxydextran chips. Three injections of 0.5 μg/ml NOD1 (*A*) or 0.5 μg/ml LRR-truncated NOD1 (*B*) were performed prior to subsequent SPR measurement and further loadings. Adsorption of NOD1 resulted in a laser deflection of 72 mDeg, corresponding to loading of 720 pg/mm^2 (*A*). Adsorption of NOD1 without the LRR domain caused a laser deflection of 42 mDeg, corresponding to a loading of 420 pg/mm^2 (*B*). *C*, after adsorption, injection of 1 M ethanolamine removed excess carboxydextran. Representative traces of four independent experiments are shown.

3, shows the height difference (Δz) between the two regions, z' and z, described above. All AFM experiments were conducted in triplicate, and the measurement of the height of the protein layer was statistically valid (Fig. 2).

We first measured the thickness of the carboxydextran film bound to the gold surface, Δz_A (Fig. 2*A*, *columns 1*, *2*, and *3*), which was found to be 4.7 ± 0.4 nm. The thickness of the carbxydextran/NOD1 layer (Δz_B) was 14.7 ± 0.7 nm (Fig. 2*B*, *columns 1*, *2*, and *3*), carboxydextran/NOD1/Tri-DAP (Δz_C) was 23.0 ± 1.0 (Fig. 2*C*, *columns 1*, *2*, and *3*), and carboxydextran/NOD1/Tri-DAP/RICK (Δz_D) was 50.4 ± 0.7 (Fig. 2*D*, *columns 1*, *2*, and *3*). To confirm that the LRR domain directly affected the interaction between NOD1 and Tri-DAP, we coated a gold chip with NOD1 and LRR-truncated NOD1. Next, Tri-DAP (Fig. 2*E*, *columns 1*, *2*, and *3*) or buffer (Fig. 2*F*, *columns 1*, *2*, and *3*) was injected onto the chip. The Δz_E and Δz_F values, the film thicknesses of LRR-truncated NOD1 with Tri-DAP and LRR-truncated NOD1 with buffer, were 37.28 ± 2.03 and 36.98 ± 3.17 nm, respectively. These results confirm that, unlike full-length NOD1, LRR-truncated NOD1 was not able to interact with Tri-DAP to form protein multilayers.

The precise height of the adsorbed protein layers is partially dependent on the relative hydration of the biopolymers. Given these limitations, the current data suggest that the NOD1 protein layer is ~10 nm, the height of Tri-DAP is ~8 nm, and the height of RICK is ~27 nm. The thickness values of AFM measurements were large compared with the size of single molecules interacting side by side; therefore, we hypothesized that the establishment of protein multilayers or hydration of the protein may be occurring.

The increase in thickness of the NOD1 layer upon binding of Tri-DAP cannot simply be explained by a "side-to-side" interaction of the two molecules. The exact nature of the change may be explained by the establishment of intermolecular interactions of NOD1 caused by Tri-DAP, such as protein multilayer establishment using Tri-DAP to stabilize the multilayer conformation; however, these hypotheses may be difficult to characterize. The alteration may modify NOD1 activity because the tridimensional structure of the protein likely affects its interactions with downstream effectors, such as RICK. As a control, we showed that the carboxydextran/NOD1/MDP layer was of a thickness similar to that of carboxydextran/NOD1, confirming the absence of direct binding between NOD1 and MDP (21.75 ± 1.87 nm). Together, the AFM measurements confirm the interaction detected by SPR and also show that MDP does not bind to NOD1. Importantly, the AFM data suggest that Tri-DAP interacts with the LRR domain of NOD1. To confirm this, we used SPR to characterize the kinetics of interaction between Tri-DAP and NOD1 and to demonstrate the key role played by the LRR domain in this interaction.

Immobilization of NOD1 and NOD1 without LRR Domain on Carboxydextran Sensor Chip—To date, no quantitative data on binding and/or interaction between molecules involved in the NOD1 signaling pathway have been obtained. To study binding

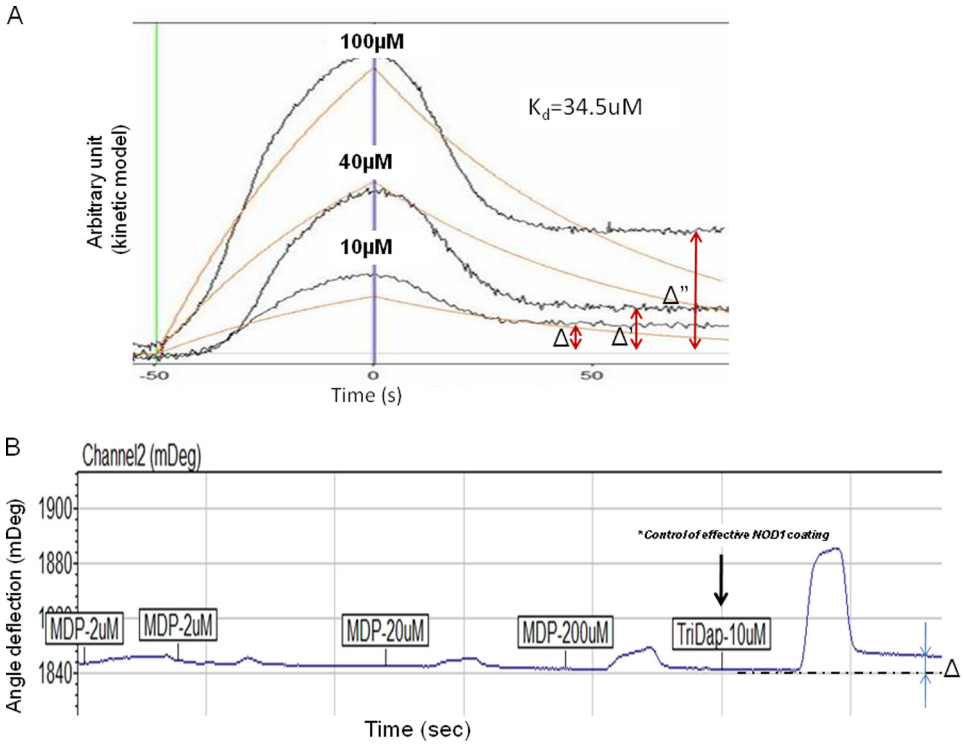

FIGURE 4. **Tri-DAP interacts directly with NOD1 protein.** *A*, determination of the K_d value of the NOD1/Tri-DAP interaction (34.5 μM) using an SPR sensorgram showing the binding of Tri-DAP (10, 20, or 100 μM) to immobilized NOD1. Experimental curves are shown in *black* for three different concentrations of CM, whereas the computational curves are shown in *red* and are fitted to the calculated kinetic constants. *B*, SPR sensorgram showing the absence of binding of circulating MDP peptide (2, 20, and 200 μM) to immobilized NOD1. As a control to confirm efficient coating of the chip with NOD1, the final experimental step confirmed successful binding of the Tri-DAP peptide to the gold chip. Representative traces of four independent experiments are shown.

between NOD1 and Tri-DAP, we used SPR (23–25). Each gold biosensor chip covered with carboxydextran was activated using a 1-ethyl-3-(3-dimethylaminopropyl) carbodiimide/*N*-hydroxysuccinimide mixture to form amide linkages between a purified protein and the chip. As shown in Fig. 3, three successive injections of 0.5 μg/ml recombinant GST-NOD1 (Fig. 3*A*, denoted as *NOD1*) or 0.5 μg/ml recombinant GST-tagged NOD1 without the LRR domain (Fig. 3*B*, shown as *CARD4*) were performed to ensure that covalent protein linkage to the chip was adequate for conducting SPR binding experiments. Linkage of recombinant proteins may be quantified by measuring the SPR resonance angle change (Δ); this is directly dependent on the number of bound molecules regardless of molecular weight or molecular length. As shown in Fig. 3*A*, linkage of NOD1 created an SPR resonance angle change of 72 mDeg, corresponding to 720 pg/mm^2 immobilized NOD1 (because 0.1 mDeg = 1 pg/mm^2). Linkage of NOD1 without the LRR domain resulted in an SPR resonance angle change of 42 mDeg, equivalent to 420 pg/mm^2 immobilized protein (Fig. 3*B*). After linkage of the two proteins, injection of 1 M ethanolamine removed unreacted carboxydextran (Fig. 3*C*). Thus, the chip was optimally coated with NOD1, and no further covalent bond could be formed between an analyte and the chip.

Tri-DAP Interacts Directly with NOD1 Protein—Tri-DAP is known to be a natural ligand of NOD1 (6, 17, 18, 28, 29). However, the direct interaction between Tri-DAP and NOD1 has not been studied, and the binding constant of the reaction remains unknown. Here, we directly examined receptor/ligand interactions using SPR. The assays were performed using NOD1 as the bound receptor and Tri-DAP at three different concentrations (10, 40, and 100 μM) as the ligand (analyte). Kinetic binding data were obtained (Fig. 4*A*). Tri-DAP (at all three concentrations) bound directly to the immobilized NOD1, and the extent of the SPR resonance angle change was related to Tri-DAP concentration. Thus, the SPR resonance angle change was 8.8 mDeg for 10 μM Tri-DAP, 27.5 mDeg for 40 μM, and 69.7 mDeg for 100 μM. The calculated equilibrium affinity (K_d value) for Tri-DAP was 35.5 μM, thus in the range typical of protein/small peptide interactions (30–32). However, we were unable to estimate whether immobilized NOD1 density on the biosensor chip was of the same order of magnitude at which physiologically relevant levels of NOD1 are expressed intracellularly. In addition, we could not explore the possible relevance that NOD1 can act cellularly in either the monomer or dimer form (33), which could affect the calculation of the binding constant of Tri-DAP/NOD1 as the software assumes a 1:1 stoichiometric ratio to calculate binding constants. Obviously, binding constants might also be affected by the covalent nature of the bond between NOD1 and the gold chip; such binding restricts NOD1 motion during interaction with Tri-DAP or RICK. The effect of motion restriction may be attenuated by the application of several passages of solutions containing free Tri-DAP or RICK, which would increase the probability of interaction. In short, our calculated K_d value may differ slightly from that which would be obtained in a more physiological environment. We repeated the experiment using the dipeptide MDP, a NOD2 ligand, as a negative control. As shown in Fig. 4*B*, MDP did not bind to NOD1 even at a passage con-

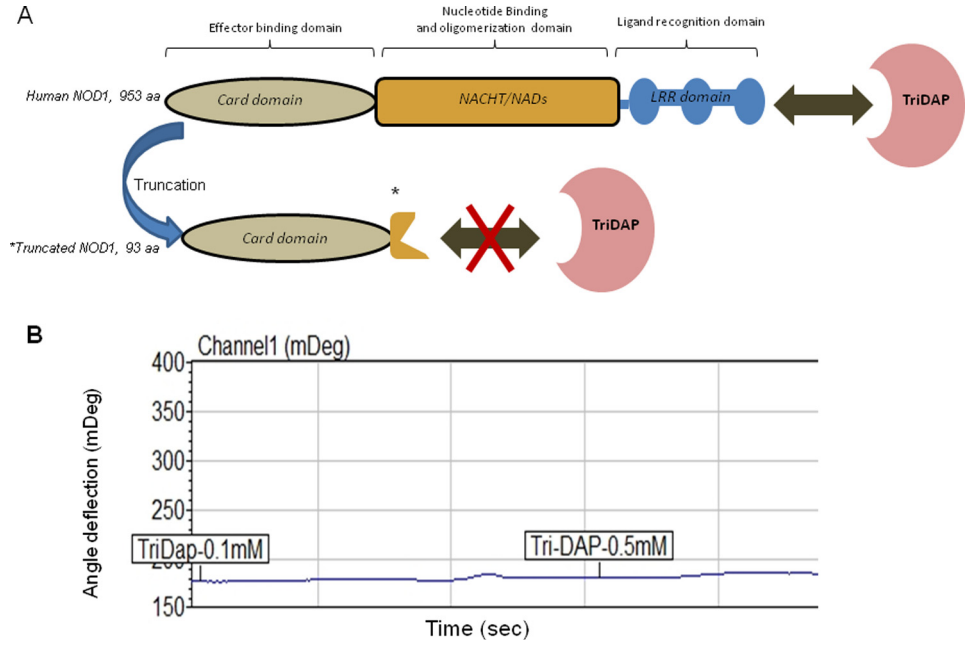

FIGURE 5. **Tri-DAP does not interact with NOD1 protein lacking LRR domain.** *A*, schematic representation of the effect of LRR truncation on Tri-DAP binding to NOD1. *B*, SPR sensorgram showing the absence of binding of circulating Tri-DAP peptide (100, 500, and 1,000 μM) to adsorbed LRR-truncated NOD1. No K_d calculation was possible below 1 mM. *aa*, amino acids.

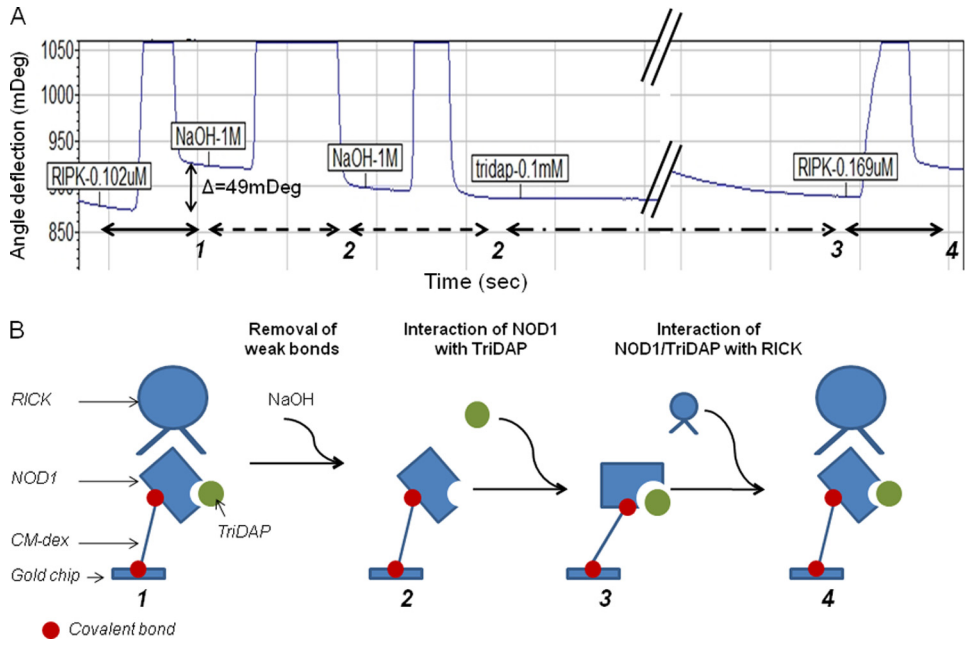

FIGURE 6. **RICK binds to Tri-DAP/NOD.** *A*, *1*, RICK (0.102 μM) bound to the NOD1·Tri-DAP complex resulting in a laser deflection of 49 mDeg. *2*, regeneration of the initial conditions by removing adsorbed RICK and Tri-DAP by treatment with 1 M NaOH. *3*, injection of 0.1 mM Tri-DAP onto a chip precoated with NOD1. *4*, injection of RICK (169 nM) onto a chip precoated with NOD1 associated with Tri-DAP. Representative traces of four independent experiments are shown. *B*, schematic representation of a typical experiment. *CM-dex*, carboxymethyldextran.

centration of 200 μM. The lack of binding was not caused by loss of chip integrity during MDP flow because subsequent Tri-DAP (10 μM) flow induced an SPR resonance angle change (9 mDeg). Together, the results show that Tri-DAP, but not MDP, binds directly to NOD1.

Tri-DAP Does Not Interact with NOD1 Protein Lacking LRR Domain—As shown schematically in Fig. 5*A*, the C-terminal LRR of NOD1 is required for recognition of Tri-DAP (34, 35). However, the studies that support this view have taken indirect approaches toward the demonstration of such interactions. The most relevant evidence comes from measurements of effects on downstream signaling pathways, such as NF-κB activation, in transfected cells containing NOD1 constructs (with or without the LRR domain) that were prestimulated with Tri-DAP (17, 36). In the present work, we directly measured interactions between Tri-DAP and NOD1 (with or without the LRR domain) using SPR. We used GST-NOD1 without the LRR domain bound to a biosensor chip and Tri-DAP at three differ-

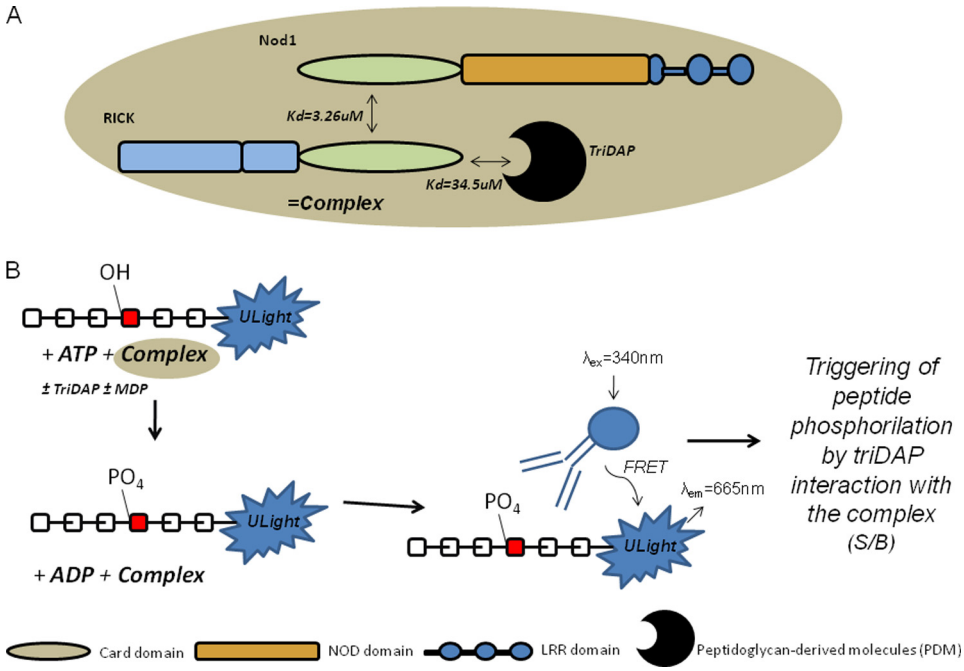

FIGURE 7. **Schematic representation of kinase assay performed to measure phosphorylation rate.** Each plot is a signal-to-background (*S/B*) ratio (signal at 665 nm/control signal (minus ATP signal at 665 nm)) obtained using four different peptides in association with NOD1·RICK·Tri-DAP complexes.

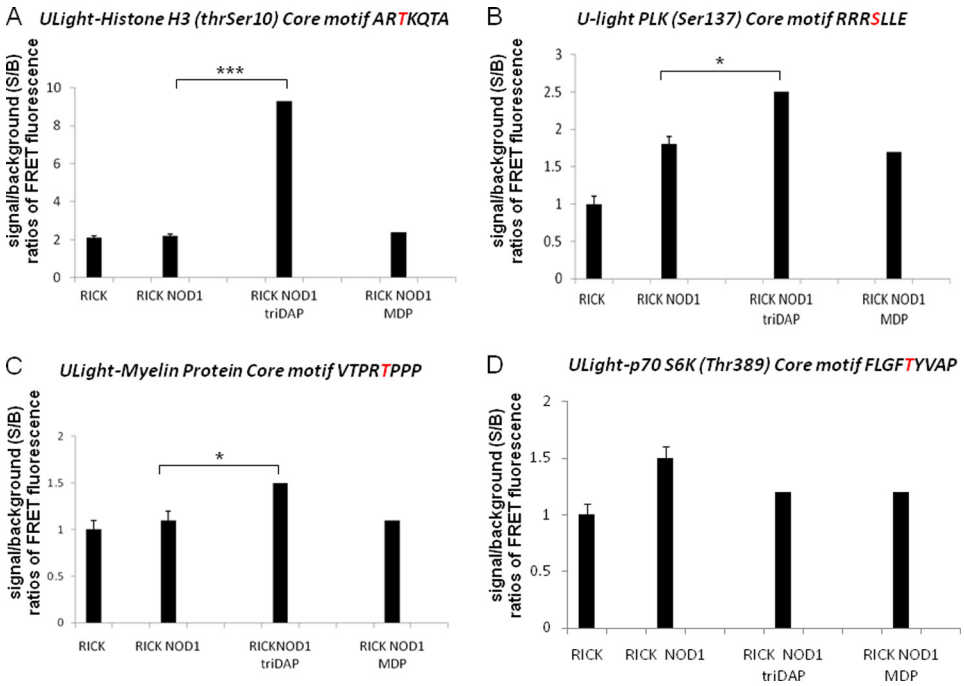

FIGURE 8. **Binding of Tri-DAP to NOD1 increases RICK phosphorylation activity.** Differential phosphorylation activity on peptide substrates (*A*, histone H3 peptides; *B*, the core motif RRRSLL; *C*, the core motif RRRSLLE; *D*, the core motif VTPRTPPP) is shown. Peptide phosphorylation sites are shown in *red*. RICK kinase was used either alone or associated with NOD1, with NOD1 in the presence of Tri-DAP, or with NOD1 in the presence of MDP. FRET fluorescence data are shown as signal-to-background (*S/B*) ratios (signal at 665 nm/control signal (minus ATP signal at 665 nm)). Values represent means ± standard error (S.E.) of $n = 3$/group. *, $p < 0.05$; ***, $p < 0.001$. *PLK*, polo-like kinase.

ent concentrations (100 μM, 500 μM, and 1 mM) to explore the interaction with NOD1. As shown in Fig. 5*B*, Tri-DAP never bound to immobilized NOD1 protein lacking the LRR domain, and a binding constant could not be calculated. Thus, the data directly show that the C-terminal LRR of NOD1 is required for recognition of Tri-DAP in agreement with previous reports (34, 35).

Tri-DAP/NOD1 Interaction Elevates Binding of NOD1 to RICK—It has been reported that NOD1 physically associates with RICK (in the RIPK2·RIP2·CARDIAK complex), a CARD-containing protein kinase, via a homophilic CARD/CARD interaction (Fig. 1*A*) (34, 37, 38). To date, the interaction between NODs (including NOD1 and NOD2) and RICK has been studied by both co-immunoprecipitation and mutagene-

sis techniques (26). However, no direct kinetic determination of the NOD1/RICK binding has been reported. First, by examining SPR resonance angle change in the present work, we found that RICK at three different concentrations (0.05, 0.169, and 0.4 μM) bound to Tri-DAP associated with immobilized NOD1. For example, RICK (0.102 μM) (Fig. 6*A*, noted as *RIPK*) binding to the NOD1·Tri-DAP complex caused an SPR resonance angle change of 49 mDeg (Fig. 6*A*). In Fig. 6*A*, large peaks representing an SPR resonance angle change were truncated for presentation purposes. Large peaks were obtained because of the high bulk refractive index changes between PBS and the molecule solvent. A schematic illustration of our experimental SPR design is shown in Fig. 6*B*. After coating of NOD1 onto the carboxydextran chip, Tri-DAP (0.1 mM) was bound upon a single injection. Once the peptide was bound, solutions with different concentrations of RICK were injected, and we measured the interaction of the NOD1·Tri-DAP complex with RICK. We performed binding experiments in the presence or absence of Tri-DAP (0.1 mM) bound to immobilized NOD1 before injection of RICK (0.05, 0.169, or 0.4 μM) as an analyte. Interestingly, binding of RICK to NOD1 reduced the SPR resonance angle change when Tri-DAP was not associated with NOD1. For example, when 0.169 μM RICK was used, the SPR resonance angle change between NOD1 and RICK in the presence of Tri-DAP was 42 *versus* 34 mDeg in the absence of Tri-DAP. The calculated equilibrium affinity (the K_d value) of RICK binding to NOD1 was 3.26 μM in the presence of Tri-DAP and 4.13 μM in the absence of the peptide. Together, these results show that binding of Tri-DAP to NOD1 increases the binding affinity between NOD1 and RICK in a synergistic manner. These results are in agreement with the notion that Tri-DAP may initiate cascade events after binding to NOD1. In this context, an increase in the binding affinity of NOD1 to RICK may be essential to amplify signal transduction to downstream protein partners involved in the signaling pathway.

Binding of Tri-DAP to NOD1 Increases RICK Phosphorylation Activity—We have shown herein that the interaction between NOD1 and RICK was stronger when Tri-DAP was bound to the LRR domain of NOD1 (Fig. 7*A*). Next, we investigated the influence of diverse protein interactions on phosphorylation activity. To explore RICK-mediated phosphorylation, we used the LANCE assay (PerkinElmer Life Sciences). Notably, the LANCE kit allows the study of RICK phosphorylation activity via the use of four distinct consensus substrate peptides (the peptides are representative of most phosphorylated protein motifs in eukaryotic cells). The assay uses FRET technology to measure fluorescence transfer between an antibody binding to a phosphorylated moiety and a ULight motif attached to the relevant peptide (Fig. 7*B*). Our results (Fig. 8) showed that the presence of Tri-DAP significantly increased phosphorylation of the peptide ULight-histone H3 (Thr-3/Ser-10) core motif ARTKQTA (Fig. 8*A*). This peptide was phosphorylated 5-fold more efficiently by the NOD1·RICK complex if Tri-DAP was present. On the other hand, MDP peptide, which does not bind NOD1, did not significantly modify RICK phosphorylation activity. Of the other three peptides tested, only two (ULight-polo-like kinase (Ser-137) core motif RRRSLLE and ULight-myelin protein core motif VTPRTPPP) showed slight increases in phosphorylation (Fig. 8, *B*, *C*, and *D*). Thus, these results show that binding of Tri-DAP to the LRR domain of NOD1 plays a key role in regulating downstream events triggered by stimulation of the PepT1-NOD1 signaling pathway.

Previous data support that Tri-DAP is transported by PepT1 into intestinal epithelial cells (1, 2, 7, 27). Once in the cytosol, Tri-DAP binds directly to the LRR domain of NOD1. Tri-DAP/NOD1 interactions increase the affinity of subsequent NOD1/RICK binding and elevate RICK phosphorylation activity. Thus, RICK phosphorylation activity is modulated by the PepT1 substrate Tri-DAP through a higher affinity binding with NOD1.

Conclusions—We have shown that Tri-DAP interacts directly with the LRR domain of NOD1 and consequently increases RICK/NOD1 association and RICK phosphorylation activity.

REFERENCES

1. Charrier, L., Driss, A., Yan, Y., Nduati, V., Klapproth, J. M., Sitaraman, S. V., and Merlin, D. (2006) *Lab. Invest.* **86,** 490–503
2. Buyse, M., Charrier, L., Sitaraman, S., Gewirtz, A., and Merlin, D. (2003) *Am. J. Pathol.* **163,** 1969–1977
3. Vavricka, S. R., Musch, M. W., Chang, J. E., Nakagawa, Y., Phanvijhitsiri, K., Waypa, T. S., Merlin, D., Schneewind, O., and Chang, E. B. (2004) *Gastroenterology* **127,** 1401–1409
4. Dalmasso, G., Nguyen, H. T., Charrier-Hisamuddin, L., Yan, Y., Laroui, H., Demoulin, B., Sitaraman, S. V., and Merlin, D. (2010) *Am. J. Physiol. Gastrointest. Liver Physiol.* **299,** G687–G696
5. Chamaillard, M., Hashimoto, M., Horie, Y., Masumoto, J., Qiu, S., Saab, L., Ogura, Y., Kawasaki, A., Fukase, K., Kusumoto, S., Valvano, M. A., Foster, S. J., Mak, T. W., Nuñez, G., and Inohara, N. (2003) *Nat. Immunol.* **4,** 702–707
6. Girardin, S. E., Travassos, L. H., Hervé, M., Blanot, D., Boneca, I. G., Philpott, D. J., Sansonetti, P. J., and Mengin-Lecreulx, D. (2003) *J. Biol. Chem.* **278,** 41702–41708
7. Merlin, D., Steel, A., Gewirtz, A. T., Si-Tahar, M., Hediger, M. A., and Madara, J. L. (1998) *J. Clin. Investig.* **102,** 2011–2018
8. Zucchelli, M., Torkvist, L., Bresso, F., Halfvarson, J., Hellquist, A., Anedda, F., Assadi, G., Lindgren, G. B., Svanfeldt, M., Janson, M., Noble, C. L., Pettersson, S., Lappalainen, M., Paavola-Sakki, P., Halme, L., Färkkilä, M., Turunen, U., Satsangi, J., Kontula, K., Löfberg, R., Kere, J., and D'Amato, M. (2009) *Inflamm. Bowel Dis.* **15,** 1562–1569
9. Daniel, H., and Kottra, G. (2004) *Pflugers Arch.* **447,** 610–618
10. Girardin, S. E., Tournebize, R., Mavris, M., Page, A. L., Li, X., Stark, G. R., Bertin, J., DiStefano, P. S., Yaniv, M., Sansonetti, P. J., and Philpott, D. J. (2001) *EMBO Rep.* **2,** 736–742
11. Lee, J., Tattoli, I., Wojtal, K. A., Vavricka, S. R., Philpott, D. J., and Girardin, S. E. (2009) *J. Biol. Chem.* **284,** 23818–23829
12. Masumoto, J., Yang, K., Varambally, S., Hasegawa, M., Tomlins, S. A., Qiu, S., Fujimoto, Y., Kawasaki, A., Foster, S. J., Horie, Y., Mak, T. W., Núñez, G., Chinnaiyan, A. M., Fukase, K., and Inohara, N. (2006) *J. Exp. Med.* **203,** 203–213
13. Viala, J., Chaput, C., Boneca, I. G., Cardona, A., Girardin, S. E., Moran, A. P., Athman, R., Mémet, S., Huerre, M. R., Coyle, A. J., DiStefano, P. S., Sansonetti, P. J., Labigne, A., Bertin, J., Philpott, D. J., and Ferrero, R. L. (2004) *Nat. Immunol.* **5,** 1166–1174
14. Watanabe, T., Asano, N., Kitani, A., Fuss, I. J., Chiba, T., and Strober, W. (2010) *Int. J. Inflam.* **2010,** 476482
15. Yao, X., Li, X., Toledo, F., Zurita-Lopez, C., Gutova, M., Momand, J., and Zhou, F. (2006) *Anal. Biochem.* **354,** 220–228
16. Lahiri, J., Isaacs, L., Grzybowski, B., Carbeck, J. D., and Whitesides, G. M. (1999) *Langmuir* **15,** 7186–7198
17. van Heel, D. A., Ghosh, S., Butler, M., Hunt, K., Foxwell, B. M., Mengin-

Lecreulx, D., and Playford, R. J.(2005) *Eur. J. Immunol.* **35,** 2471–2476
18. Enoksson, M., Ejendal, K. F., McAlpine, S., Nilsson, G., and Lunderius-Andersson, C. (2011) *J. Innate Immun.* **3,** 142–149
19. Inohara, N., and Nuñez, G. (2001) *Oncogene.* **20,** 6473–6481
20. Inohara, N., and Nuñez, G. (2003) *Nat. Rev. Immunol.* **3,** 371–382
21. Kufer, T. A., Banks, D. J., and Philpott, D. J. (2006) *Ann. N.Y. Acad. Sci.* **1072,** 19–27
22. Zhu, R., Ebner, A., Kastner, M., Preiner, J., Howorka, S., and Hinterdorfer, P. (2009) *Chemphyschem* **10,** 1478–1481
23. Torreri, P., Ceccarini, M., Macioce, P., and Petrucci, T. C. (2005) *Ann. Ist. Super. Sanita* **41,** 437–441
24. Vollmer, W., von Rechenberg, M., and Höltje, J. V. (1999) *J. Biol. Chem.* **274,** 6726–6734
25. Amano, A., Nakamura, T., Kimura, S., Morisaki, I., Nakagawa, I., Kawabata, S., and Hamada, S. (1999) *Infect. Immun.* **67,** 2399–2405
26. Ogura, Y., Inohara, N., Benito, A., Chen, F. F., Yamaoka, S., and Nunez, G. (2001) *J. Biol. Chem.* **276,** 4812–4818
27. Merlin, D., Si-Tahar, M., Sitaraman, S. V., Eastburn, K., Williams, I., Liu, X., Hediger, M. A., and Madara, J. L. (2001) *Gastroenterology* **120,** 1666–1679
28. van Heel, D. A., Hunt, K. A., Ghosh, S., Hervé, M., and Playford, R. J. (2006) *Eur. J. Immunol.* **36,** 1629–1635
29. van Heel, D. A., Hunt, K. A., Ghosh, S., Hervé, M., and Playford, R. J. (2005) *Gut* **54,** 1553–1557
30. O'Shannessy, D. J. (1994) *Curr. Opin. Biotechnol.* **5,** 65–71
31. O'Shannessy, D. J., Brigham-Burke, M., Soneson, K. K., Hensley, P., and Brooks, I.(1994) *Methods Enzymol.* **240,** 323–349
32. O'Shannessy, D. J., Brigham-Burke, M., Soneson, K. K., Hensley, P., and Brooks, I. (1993) *Anal. Biochem.* **212,** 457–468
33. Srimathi, T., Robbins, S. L., Dubas, R. L., Hasegawa, M., Inohara, N., and Park, Y. C. (2008) *Biochemistry* **47,** 1319–1325
34. Inohara, N., Chamaillard, M., McDonald, C., and Nuñez, G. (2005) *Annu. Rev. Biochem.* **74,** 355–383
35. Dziarski, R. (2003) *Cell. Mol. Life Sci.* **60,** 1793–1804
36. Uehara, A., Yang, S., Fujimoto, Y., Fukase, K., Kusumoto, S., Shibata, K., Sugawara, S., and Takada, H. (2005) *Cell. Microbiol.* **7,** 53–61
37. Manon, F., Favier, A., Núñez, G., Simorre, J. P., and Cusack, S. (2007) *J. Mol. Biol.* **365,** 160–174
38. Inohara, N., Koseki, T., Lin, J., del Peso, L., Lucas, P. C., Chen, F. F., Ogura, Y., and Núñez, G. (2000) *J. Biol. Chem.* **275,** 27823–27831

l-Ala-γ-d-Glu-*meso*-diaminopimelic Acid (DAP) Interacts Directly with Leucine-rich Region Domain of Nucleotide-binding Oligomerization Domain 1, Increasing Phosphorylation Activity of Receptor-interacting Serine/Threonine-protein Kinase 2 and Its Interaction with Nucleotide-binding Oligomerization Domain 1

Hamed Laroui, Yutao Yan, Yoshie Narui, Sarah A. Ingersoll, Saravanan Ayyadurai, Moiz A. Charania, Feimeng Zhou, Binghe Wang, Khalid Salaita, Shanthi V. Sitaraman and Didier Merlin

J. Biol. Chem. 2011, 286:31003-31013.
doi: 10.1074/jbc.M111.257501 originally published online July 12, 2011
